

# Experimental verification of EUV mask limitations at high numerical apertures

Rikon Chao<sup>1,2</sup>, Paul Graeupner<sup>3</sup>, Eric Gullikson<sup>1</sup>, Seong-Sue Kim<sup>4</sup>, Jens-Timo Neumann<sup>3</sup>, Ryan Miyakawa<sup>1</sup>, Hwan-Seok Seo<sup>4</sup>, Andy Neureuther<sup>2</sup>, and Patrick Naulleau<sup>1</sup>

<sup>1</sup>Center for X-ray Optics, Lawrence Berkeley National Laboratory, Berkeley, CA, 94720

<sup>2</sup>Department of EECS, University of California, Berkeley, CA 94720

<sup>3</sup>Carl Zeiss SMT GmbH, Rudolf-Eber-Str. 2, 73447 Oberkochen, Germany

<sup>4</sup>Samsung Electronics Co., Ltd., Hwasung, Gyeonggi 445-701, Korea

## ABSTRACT

In this work, we use a high accuracy synchrotron-based reflectometer to experimentally determine the effects of angular bandwidth limitations on high NA EUV performance. We characterized mask blank and mask pattern diffraction performance as a function of illumination angle, scatter angle, and wavelength. A variety of pattern feature sizes ranging down to coded sizes of 11 nm (44 nm on the mask) are considered. A Rigorous Coupled-Wave Analysis (RCWA) model is calibrated against the experimental data to enable future model-based performance predictions. The model is optimized against the clearfield data and verified by predicting the mask pattern diffraction data. We thus have confirmed the degradation and asymmetry of diffraction orders at high AOI.

**Keywords:** Angular bandwidth, Extreme ultraviolet lithography, Modeling, Multilayers, Reflectivity

## 1. INTRODUCTION

To meet future scaling needs, extreme ultraviolet (EUV) lithography is expected to be extended to numerical apertures (NAs) of 0.45 and beyond. The reflective nature of EUV masks, however, requires the angle of incidence (AOI) to be higher than what is currently being used if high NA systems are adopted. Assuming a magnification of 4x would require a mean illumination angle of 9 degrees at the mask. If an AOI of 9 degrees is used with a partial coherence of unity, and an NA of 0.5, the maximum AOI encountered is

$$AOI_{max} = 9 + \sin^{-1} \frac{0.5}{4} = 16.2 \quad (1)$$

At such a high incident angle, there are two effects limiting the performance of an EUV mask, angular bandwidth and mask shadowing. The former effect describes the dropping of reflectivity at incident angle far beyond the optimized angle. This can be compensated for at the sacrifice of reflectivity at lower angles, with a different design of the broadband multilayer stack [1]. The latter effect, mask shadowing, can in theory be mitigated by thinning the absorber layer [2], but this would in turn be limited by the absorption performance. Simulation work showed that it is possible to have either good imaging contrast or reasonable efficiency, but not both [3]. This drove the authors of [3] to the conclusion that a higher NA ( $\gg 0.33$ ) is only possible if accompanied by an increased demagnification in order to reduce the AOI at the reticle. It thus becomes important to experimentally determine how the limitations affect the diffraction performance.

This paper begins with a description of a test mask. Measurement details are then given, followed by the methodology of calibration of the stack parameters. The calibrated modeled was used to predict the reflectivity on clear field and absorber field, and compared with the measurement. Measured data and modeling from line and space patterns on mask are then reported. Implications for various incident angles, mask pitches, duty cycles as well as the deviation of this data from that of an ideal thin-mask is finally discussed.

## 2. FIRST ROUND MEASUREMENT AND MODELING

### 2.1 Mask layout

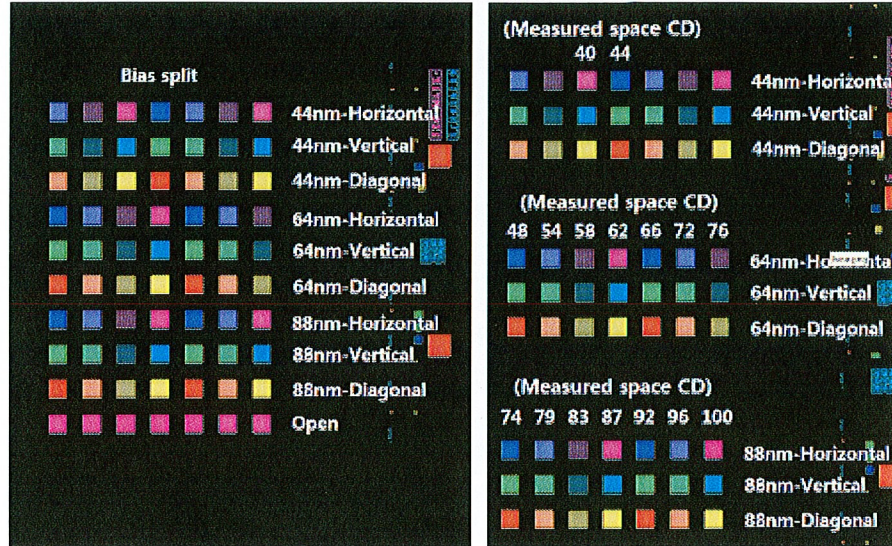


Figure 1. Designed layout of the mask to be measured. This includes three different pitches in three orientations and clear field windows (noted as “open”). For each particular pitch and orientation, a few biases on space CD are chosen to fabricate.

As shown in Figure 1, we designed a mask of multilayer/capping/absorber layers with two types of windows: clear field windows, on which only multilayers capped with Ruthenium are present, and patterned areas, where absorber line-and-space gratings were deposited on top of the capping layer. Regions other than those were filled with absorber. The multilayer is composed of 40 pairs of Si/Mo bilayers. For the gratings, lines and spaces of three different pitches (88, 128, and 176 nm) combined with three orientations (horizontal, vertical, and diagonal) were made, which were used to measure the diffraction orders. For each of the pitches, a few biases were added as shown in the figure. The purpose of the clear fields was to measure reflectivity of mask blank, against which the parameters would be calibrated with rigorous coupled wave analysis (RCWA). The absorber parameters would then be calibrated against measurement on unopened absorber regions with the same method.

### 2.2 Measurement

Reflectivity and scattering measurements were performed using the synchrotron-based reflectometer of the Calibrations and Standards Beamline 6.3.2 at Advanced Light Source (ALS), Lawrence Berkeley National Laboratory (LBNL). The beamline has a high spectral purity of 99.98%, wavelength precision of 0.007%, and a reflectance precision of 0.08% [4]. Reflectivity on clear field and absorber field was measured at angles of incidence (AOI) of 2, 4, 6, 8, 9, 10, 12, 14, and 16 degrees, and the wavelength spanned from 13.3 nm to 13.7 nm with steps of 0.05 nm. Detector angles were set at the same angles of AOI but on the other side. For scattering measurement, data was collected at the same set of AOI and wavelengths, but the detector was positioned at angles where scattered orders occur. The measurement was done on 8 chosen vertical grating windows (space CD/pitch): 40/88, 44/88, 58/128, 62/128, 66/128, 83/176, 87/176, and 92/176. The angles of detector  $\theta_d$  for any combination of wavelength  $\lambda$ , pitch  $d$ , and AOI  $\theta_i$ , at  $n$ th order, were precalculated using

$$n\lambda = d(\sin\theta_d - \sin\theta_i) \quad (2)$$

Scattered data was collected up to 45 degrees either side from specular, unless overlapping with incidence.

### 2.3 Calibration of parameters with optimization algorithm

The modeling work of clear field reflectivity was conducted using rigorous coupled-wave analysis (RCWA) in HyperLith [5] supported by Panoramic Technology, Inc. Initial parameters in this modeling work include pitch of Si/Mo multilayer,  $\gamma$  (ratio of Mo thickness over pitch), Ru (as capping layer) thickness, and refractive indices for Si, Mo, and

Ru. It is known that interdiffusion takes place at the Si/Mo interfaces and degrades the reflectivity performance [6]. To account for the interdiffusion effects between various layers, we added MoSi<sub>2</sub> at every Mo/Si interface in the modeling [7], and Ru<sub>2</sub>Si<sub>3</sub> at Ru/Si interface [8]. Due to possibly different amount of interdiffusion formed by the top and bottom Si and Mo, we set them as different fitting parameters. Another consideration we included is the dependency of n and k on the wavelength. Also, since phase roughness replicated through the multilayer can be another source of reflectivity reduction, we added a scaling factor that scaled down the modeling data to have a better fit with measured data.

With the support of Panoramic API, we set up automated optimization routine to calibrate the values of the parameters that would give best fit to the measured reflectivity data. Table 1 shows the measured thicknesses and refractive indices, based on which each of the parameters was assigned an initial value and a range within which it was allowed to float, as shown in Table 2. Some initial values not measured and recorded in Table 1 such as interdiffusion thicknesses were found by preliminary manual search. N and k values were corrected for different wavelengths according to differences calculated from the CXRO database [9]. We fit the clear field reflectivity first, followed by fitting of absorber field reflectivity. We hoped to find a set of parameters that best predict the measured data in terms of minimum errors.

Layer (from top)	1	2	3	Multilayer
Material	Absorber	Buffer	Capping	Si/Mo
Thickness (target)	14nm	56nm	2.5nm	40 pairs, Period=7nm, gamma=0.4 (approx.)
n (13.5nm)	0.9556	0.9492	0.9026	Si (top)=0.99901, Mo (bottom)=0.921838
k (13.5nm)	0.0232	0.0296	0.0157	Si (top)=0.001826, Mo (bottom)=0.006334
Remarks	Measured @CXRO	Measured @CXRO	Measured @CXRO	CXRO database

Table 1. Mask stack info measured at Center of X-Ray Optics (CXRO), LBNL or taken from CXRO database [9]

Parameter	Initial Value	Lower Bound	Upper Bound	Final	Source of n and k values
Scaling factor	1	0.83	1	0.9983	-
Absorber thickness (nm)	14	14*0.5	14*2	28	Measured at CXRO
Buffer thickness (nm)	56	56*0.5	56*2	57.09	
Ru thickness, clear field (nm)	1.75	0	See remark 1	4.65	
Ru thickness, absorber field (nm)	1.75	See remark 1	-	4.94	
Ru <sub>2</sub> Si <sub>3</sub> thickness	1	0	-	0.02	CXRO database
Top Si thickness (nm)	2.73	0	Pitch	2.85	
MoSi <sub>2</sub> (above Mo) thickness (nm)	1.37	0	Pitch	1.53	
Mo Thickness (nm)	1.81	0	Pitch	1.82	
MoSi <sub>2</sub> (above Si) thickness (nm)	1.09	0	Pitch	1.00	
Si thickness (nm)	2.73	0	Pitch	2.65	
Bottom Mo thickness (nm)	1.81	0	Pitch	2.33	

Remark 1: Due to possible overetching, Ru thickness on clear field can only be smaller than that on absorber field.

Table 2. List of parameters used in the optimization routine with respective ranges and the final value we arrived at to predict the diffraction.

## 2.4 Comparison of measured and modeled reflectivity

The final values that the routine arrived at gave a prediction of clear field reflectivity at various AOI as shown in Figure 2. Figure 3 shows the results when the absorber was added. The calibrated model shows a very high accuracy to the measured reflectivity at clear field, and the differences at absorber field are larger. Two parameters that arrived at a value much further than expected was Ru and absorber thicknesses, which ended up being ~ 2nm more and twice as much (stopped by the upper bound) than the measurement, respectively. The reasons remain unclear. Interdiffusion between Ru and top Si layer came to a negligible value. Other values stayed closed to what was suggested initially.

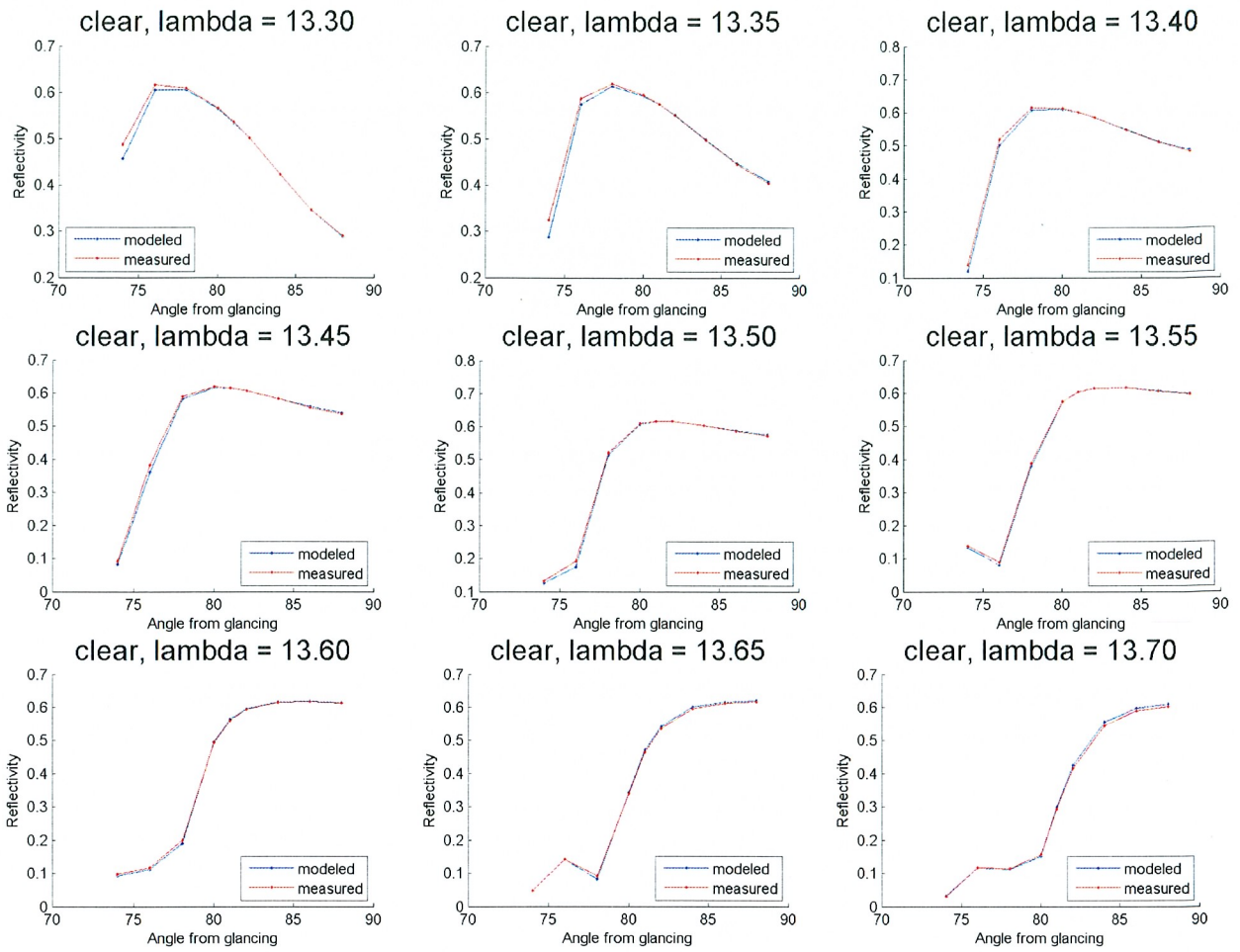


Figure 2. Clear field reflectivity of measured and modeled data. Modeling parameters are optimized for best fit to clear field based on minimum error.

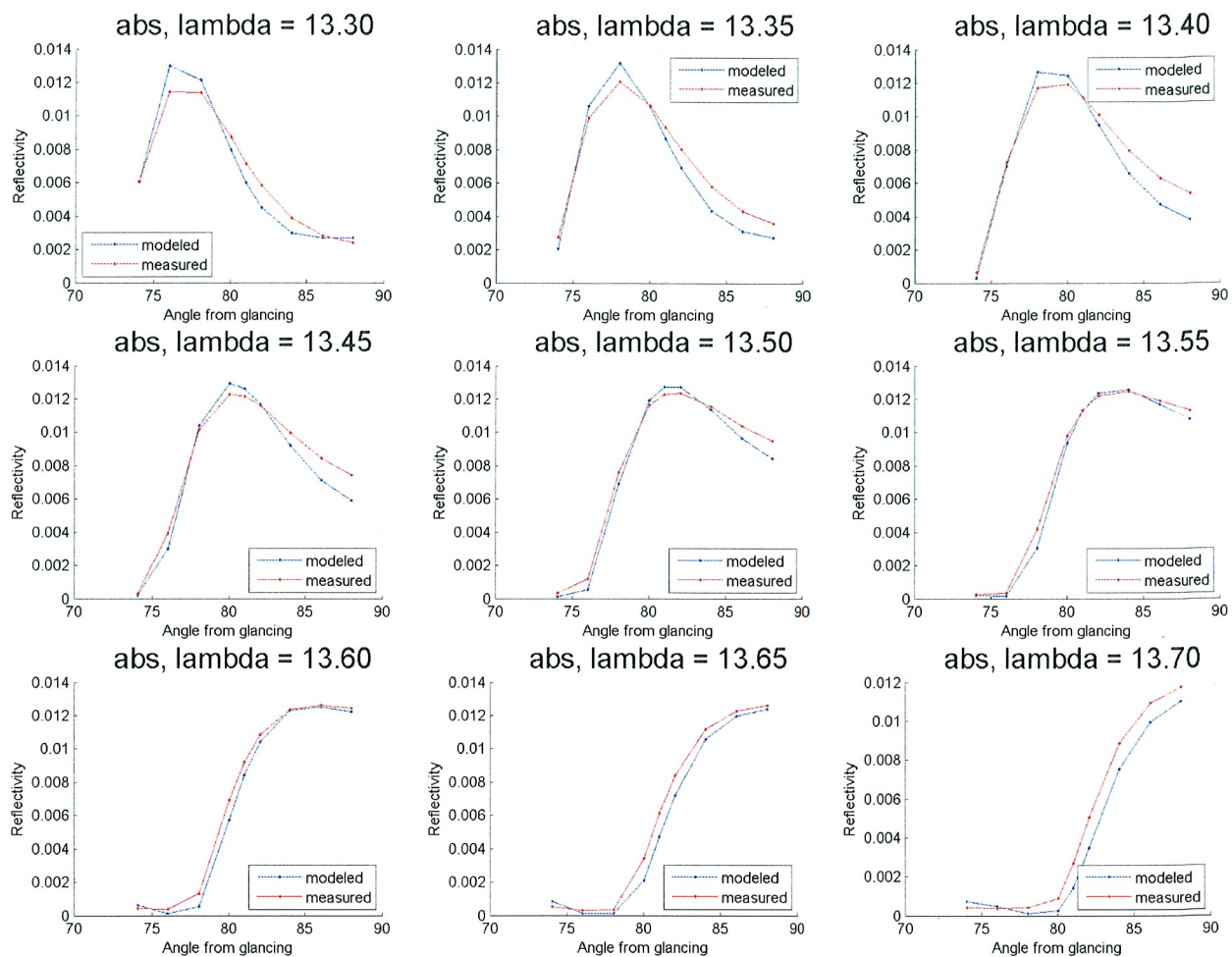


Figure 3. Absorber field reflectivity of measured and modeled data. Si/Mo stack parameters are optimized for clear field, while absorber and buffer layer parameters are optimized for absorber field based on minimum error.

## 2.5 Grating diffraction orders modeling compared with measurement

Based on the calibrated values we considered best representing the mask stack, we modeled the diffraction orders as a function of AOI, wavelength, space CDs and pitches. The model assumes the sidewall to be perfectly vertical, with no line edge roughness. Some of the results are shown in Figure 4.

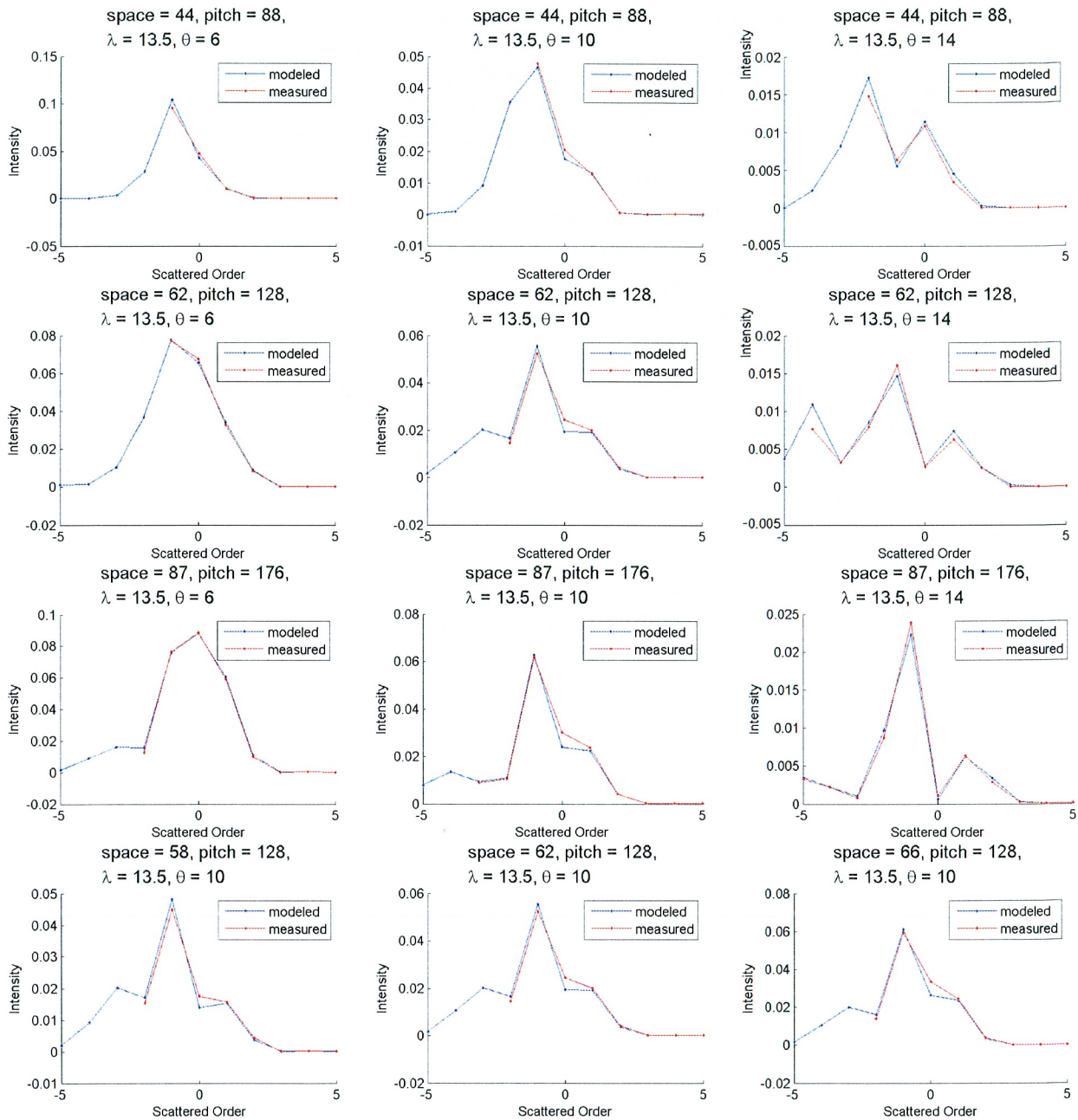


Figure 4. Selected plots showing diffraction orders measured and modeled based on calibrated parameter values in Table 2.

	-2	-1	0	1	2
44/88, 6° AOI		0.094541	0.047189	0.00995	0.000476
44/88, 14° AOI	0.014691	0.006354	0.010789	0.003369	0.000009
87/176, 6° AOI	0.012491	0.076371	0.08849	0.058877	0.009545
87/176, 14° AOI	0.008727	0.023854	0.001003	0.006319	0.00281

Table 3. Comparison of measured intensity at -2<sup>nd</sup> to 2<sup>nd</sup> orders for selected combination of pitches and AOI.

As the light is coming from an oblique angle, from the figure we can clearly see that the intensities are not symmetrical about the 0<sup>th</sup> order. However, at larger pitches and smaller AOI, the diffraction intensities show a more symmetrical profile. This is expected both due to reduced shadowing effects and the smaller angular bandwidth of the diffraction pattern. Note that the effect is also exacerbated by the fact that the multilayer is designed for an angle of incidence of 6°. In principle, one could readily optimize the multilayer d-spacing to match the AOI, but as discussed above, increasing multilayer angular bandwidth is more complicated and will come at the cost of flux. Table 3 gives the measured intensity at -2<sup>nd</sup> to 2<sup>nd</sup> orders for selected combination of pitches and AOI. Since the grating 87/176 has a duty cycle closed to 0.5,

we would expect a ratio of intensity between 0<sup>th</sup> and 1<sup>st</sup> order to be  $\left(\frac{1}{\frac{2}{1}}\right)^2 = 2.47$  for a thin mask of same CD and pitch.

However, we observed here that the measured value at 6° AOI, which should be a good estimate of a thin mask, gives  $\frac{0.08849}{0.076371} = 1.16$  and  $\frac{0.08849}{0.058877} = 1.50$  for -1<sup>st</sup> and 1<sup>st</sup> orders. This indicates loss of 0<sup>th</sup> order energy to two first orders. If we take a closer look at the grating 87/176, as the AOI increases, 0<sup>th</sup> decreases the fastest, followed by 1<sup>st</sup> order. Interestingly, -1<sup>st</sup> drops the slowest, implying a relatively strong energy. This can be explained by the fact that reflectivity at the diffracted angle of -1<sup>st</sup> order,

$$\sin^{-1}\left(\sin 14^\circ - \frac{13.5}{176}\right) = 9.51^\circ,$$

is much higher than the others, as evident from the 13.5nm case in Figure 2. On the other hand, for a fixed AOI of 6°, it is apparent that the -1<sup>st</sup> order intensity is relatively high for smaller pitches. However, this requires a different explanation since the reflectivity at this diffracted angle,

$$\sin^{-1}\left(\sin 6^\circ - \frac{13.5}{88}\right) = -2.8^\circ,$$

is similar to that at 6°. Duty cycle effects can be seen by the bottom row graphs in Figure 4. 0<sup>th</sup> order intensity increases as space CD increases, as expected since the DC term increases as more light makes it through the absorber grating. There are little effects on other orders.

It would be interesting to look at the electric field strength over diffraction orders as a function of duty cycles for the three pitches, and develop a thin mask model which helps gain insight on the magnitude and phase of reflection from the absorber. The nonzero 2<sup>nd</sup> order indicates the possible existence of EM edge effects at mask edges as in the thin-mask model the second order is zero.

### 3. CONCLUSION

In this work, we considered the imaging performance with 0.45 NA and above. To do this, gratings down to 44 nm half pitch on mask was measured by scatterometry up to 16 degrees AOI and with light wavelength ranging from 13.3 nm to 13.7 nm. After calibration against clear field and absorber field, RCWA-based modeling predicts a trend of diffraction orders similar to the measurement. We thus have confirmed the degradation and asymmetry of diffraction orders at high AOI. This complements the previous simulation studies on the mask effects by [3]. Future work will include using the calibrated model to design high-NA optimized mask architectures and experimental verification.

### ACKNOWLEDGEMENT

Software support was provided by Tom Pistor of Panoramic Technologies. This work was supported in part by Zeiss and Samsung and carried out at Lawrence Berkeley National Laboratory which is operated under the auspices of the Director, Office of Science, of the U.S. Department of Energy under Contract No. DE-AC02-05CH11231.

## REFERENCES

- [1] Ruoff, Johannes. "Impact of mask topography and multilayer stack on high NA imaging of EUV masks." SPIE Photomask Technology. International Society for Optics and Photonics, 2010.
- [2] Kim, Tae Geun, et al. "Characterization of Ru layer for capping/buffer application in EUVL mask." *Microelectronic engineering* 83.4 (2006): 688-691.
- [3] Neumann, Jens Timo, et al. "Interactions of 3D mask effects and NA in EUV lithography." *Proc. of SPIE Vol. 8522*.
- [4] The CXRO Reflectometer, <http://www.cxro.lbl.gov/reflectometer>.
- [5] Panoramic Technology, Inc., "EM-suite: core lithography simulation package," (2012), see <http://www.panoramictech.com>.
- [6] Alameda, Jennifer B., et al. "Improved reflectance and stability of Mo-Si multilayers." *Optical engineering* 41.8 (2002): 1797-1804.
- [7] Stearns, D. G., et al. "Thermally induced structural modification of Mo-Si multilayers." *Journal of applied physics* 67.5 (1990): 2415-2427.
- [8] Matsui, Y., et al. "An oxidation barrier layer for metal-insulator-metal capacitors: ruthenium silicide." *Thin solid films* 437.1 (2003): 51-56.
- [9] Henke, Burton L., E. M. Gullikson, and John C. Davis. "X-Ray Interactions: Photoabsorption, Scattering, Transmission, and Reflection at  $E = 50\text{-}30,000$  eV,  $Z = 1\text{-}92$ ." *Atomic data and nuclear data tables* 54.2 (1993): 181-342.

## **DISCLAIMER**

This document was prepared as an account of work sponsored by the United States Government. While this document is believed to contain correct information, neither the United States Government nor any agency thereof, nor The Regents of the University of California, nor any of their employees, makes any warranty, express or implied, or assumes any legal responsibility for the accuracy, completeness, or usefulness of any information, apparatus, product, or process disclosed, or represents that its use would not infringe privately owned rights. Reference herein to any specific commercial product, process, or service by its trade name, trademark, manufacturer, or otherwise, does not necessarily constitute or imply its endorsement, recommendation, or favoring by the United States Government or any agency thereof, or The Regents of the University of California. The views and opinions of authors expressed herein do not necessarily state or reflect those of the United States Government or any agency thereof or The Regents of the University of California.

This work was supported by the Director, Office of Science, of the U.S. Department of Energy under Contract No. DE-AC02-05CH11231.